Journal of Fluorine Chemistry 140 (2012) 38–42

Contents lists available at SciVerse ScienceDirect

Journal of Fluorine Chemistry

journal homepage: www.elsevier.com/locate/fluor

Synthesis and upconversion properties of Ln^{3+} doped YOF nanofibers

Renyuan Yang, Guanshi Qin, Dan Zhao, Kezhi Zheng, Weiping Qin *

State Key Laboratory on Integrated Optoelectronics, College of Electronic Science and Engineering, Jilin University, Changchun 130012, PR China

ARTICLE INFO

Article history:
Received 17 February 2012
Received in revised form 8 April 2012
Accepted 16 April 2012
Available online 27 April 2012

Keywords:
Upconversion
Electrospinning
Oxyfluoride

ABSTRACT

Nanofibers of YOF doped with trivalent lanthanide ions (Ln^{3+}) have been synthesized successfully via an electrospinning method combining with high-temperature calcination in air. Scanning electron microscopy (SEM) observations showed that the nanofibers had uniform one-dimensional (1D) morphology. X-ray diffraction (XRD) analysis and transmission electron microscopy (TEM) images revealed that the calcined fibers were constituted by rhombohedral phase yttrium oxyfluoride nanocrystals. Under the excitation from a 980 nm laser diode, YOF:Yb^{3+},Tm^{3+} and YOF:Yb^{3+},Er^{3+} fibers emitted blue and red light, respectively. Upconversion mechanisms of these YOF:Ln^{3+} fibers were also discussed in detail.

1. Introduction

Recently, one-dimensional (1D) nanomaterials, such as nanotubes [1], nanorods [2] and nanowires [3], have received much attention owing to great fundamental interests and potential applications in display, data storage, optoelectronic device, etc. [4–8]. For example, material of 1D structure is expected to be of high value to the function and integration of nanoscale devices, due to its merit of efficiently transporting electrons and optical excitations. In the past decade, various methods have been employed to develop 1D materials. Among them, electrospinning is a quite facile and efficient method to produce 1D materials. It is a manufacturing approach that uses strong electric force to draw a fluid into fine filaments which have diameters ranging from several microns down to tens of nanometers [9–16].

Polymer-based 1D materials have been developed in virtue of electrospinning [17–19]. However, in polymer-based 1D materials, polymer takes a large proportion of composite fibers and, as a result, the excited Ln^{3+} can be badly quenched due to the high-energy vibrations of polymers [20,21]. To improve properties of 1D materials, polymer ought to be removed. Pure inorganic 1D materials are expected to perform better fluorescent character than organic fibers.

To prepare pure inorganic 1D materials, an electrospinning method combining with an appropriate calcination process has been developed. As a classical procedure, composite fibers are prepared in advance containing polymer and the precursor of target substance; after a necessary calcination process, the organic contents are burned out and inorganic products form are yielded [22–26]. Recently, inorganic 1D materials of RE oxysalts and RE oxide such as YVO_4, YPO_4, YBO_3, and Gd_2O_3 have been synthesized successfully by the electrospinning-and-calcinate procedure [27–30]. Among upconversion (UC) materials, high efficient UC fluorescence can be obtained in Ln^{3+}-doped host materials with low phonon energy owing to the reduced multi-phonon relaxation rates in them [31–36]. Therefore, fluorides, which have lower phonon energy than oxides, are well known as preferable host materials for UC applications [37,38]. On the other hand, in practical applications, oxides have an advantage superior to fluorides due to their good chemical durability and excellent mechanical strength. Consequently, combining the thermal stability of oxides and the low phonon property of fluorides, oxy-fluorides have been considered in developing practical UC materials. However, many of the studies concerning Ln^{3+}-doped oxyfluorides have been focused on bulk materials like glasses and ceramics, and, to our best knowledge, there are no reports on oxyfluoride nanofibers. Hence, to synthesize 1D oxyfluoride fibers by using electrospinning technique remains a challenging task and is crucial to the development long inorganic nanofibers.

In this work, we report the synthesis and UC fluorescence properties of Ln^{3+}-doped YOF nanofibers. It is the first time to synthesize ultralong inorganic fibers of UC materials. The diameters of precursor fibers and sintered fibers were tunable from hundreds nanometers to tens nanometers. With 980 nm excitation, blue and red UC fluorescence was observed in YOF:20%Yb,0.5%Tm and YOF:20%Yb,4%Er, respectively.

2. Results and discussions

2.1. Structure and morphology

The phase evolution of the fibers sintered at different temperatures in air was evaluated by using XRD analysis. In the

* Corresponding author. Tel.: +86 431 85168241x8325; fax: +86 431 85168241x8325.
E-mail address: wpqin@jlu.edu.cn (W. Qin).

0022-1139/$ – see front matter.
http://dx.doi.org/10.1016/j.jfluchem.2012.04.009

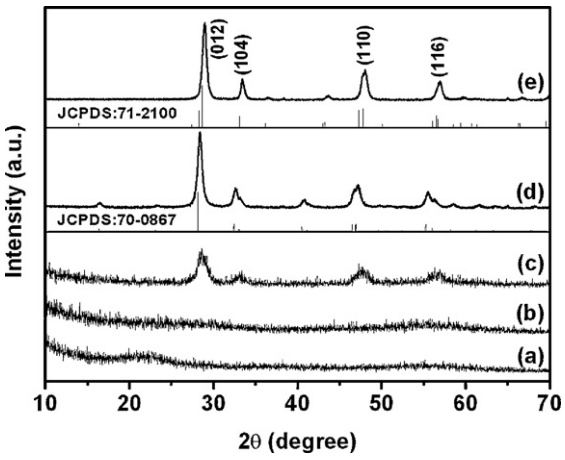

Fig. 1. XRD patterns of the fibers: (a) $RE(CF_3COO)_3$/PVP composite fibers; (b–e) samples which were sintered in air at 300 °C, 400 °C, 500 °C, and 600 °C, respectively.

XRD pattern of as-spun fibers, as shown in Fig. 1(a), the broad band ranging from 17° to 25° (2θ) is ascribed to the amorphous PVP. No trifluoroacetate phase can be found, which means that non-crystalline $RE(CF_3COO)_3$ (RE = Y, Yb) molecules have dispersed homogeneously in the composite fibers. The broad band disappears in Fig. 1(b), implying that PVP in $RE(CF_3COO)_3$/PVP composite fibers has been decomposed at 300 °C in air. The diffraction peaks of crystalline yttrium oxyfluoride appear for the sample annealed at 400 °C in air, as shown in Fig. 1(c). The intensities of the peaks in Fig. 1(d) indicate that the sample annealed at 500 °C in air is highly crystalline in nature. The peak positions correspond closely to the standard pattern of orthorhombic $Y_7O_6F_9$ (JCPDS 70-0867). Fig. 1(e) shows the XRD pattern of the sample sintered at 600 °C in air. All these peaks can be closely indexed to the rhombohedral phase of YOF according to JCPDS card (No. 71-2100). As no additional peaks for other phases can be found, we infer that Ln^{3+} ions have substituted Y^{3+} ions and been effectively doped in the YOF host lattice. The XRD patterns of Ln^{3+}-doped samples have a shift to a large angle in comparison to the standard cards, which implies that the unit-cell parameters in the Ln^{3+}-doped samples have changed by a small amount. For instance, in pattern (e) the XRD peaks of the (0 1 2) and (1 0 4) planes locate at $2\theta = 28.9°$ and 33.4°, respectively. However, in the standard card, they locate at $2\theta = 28.7°$ and 33.2°. All the three Ln^{3+} ions (Er^{3+}, Tm^{3+},Yb^{3+}) are smaller than Y^{3+} in the YOF host lattice. The calculated crystal cell parameters (a = 0.378415 nm and c = 1.870655 nm) for the crystalline YOF:Ln^{3+} fibers are smaller than the values (a = 0.379700 nm and c = 1.88900 nm) of pure YOF (JCPDS 71-2100) due to the substitution of Y^{3+} by Ln^{3+}.

The morphology and size of the precursor fibers could be influenced by various factors: voltage, distance between the tip and the collector, mass ratio of polymer in solution, relative humidity (RH), and so on. The voltage as well as the distance between spinneret tip and the collector essentially determined the electric field and therefore played a cardinal role in electrospinning process. When the electric field enhanced, the fibers became thinner. On the other hand, liquid jets would become instable and inhomogeneous fibers would be obtained in the products if the electric field was as low as 0.5 kV/cm. The average diameter of the fibers enlarged accordingly when the PVP mass ratio was increased. The PVP mass ratio of the fibers in Fig. 2(a–c) was 2.0 wt%, 2.5 wt%, and 3.0 wt%, respectively. The ideal RH for the electrospinning was less than 30%. The composite fibers in Fig. 2 were fabricated under the condition of 15 kV (voltage), 12 cm (distance), and ~20% (RH).

The $RE(CF_3COO)_3$/PVP composite fibers were calcined subsequently. Fig. 2(d) shows the SEM image of fibers calcined at 600 °C for 24 h in air. These fibers originated from the precursor fibers shown in Fig. 2(b). The annealed fibers kept their 1D morphology just like the precursor fibers presenting. Their average diameter shrank to ca. 100 nm, and their lengths were still more than hundreds of microns. In contrast, their precursor fibers had an average diameter of ca. 200 nm. In general, the use of $RE(CF_3COO)_3$

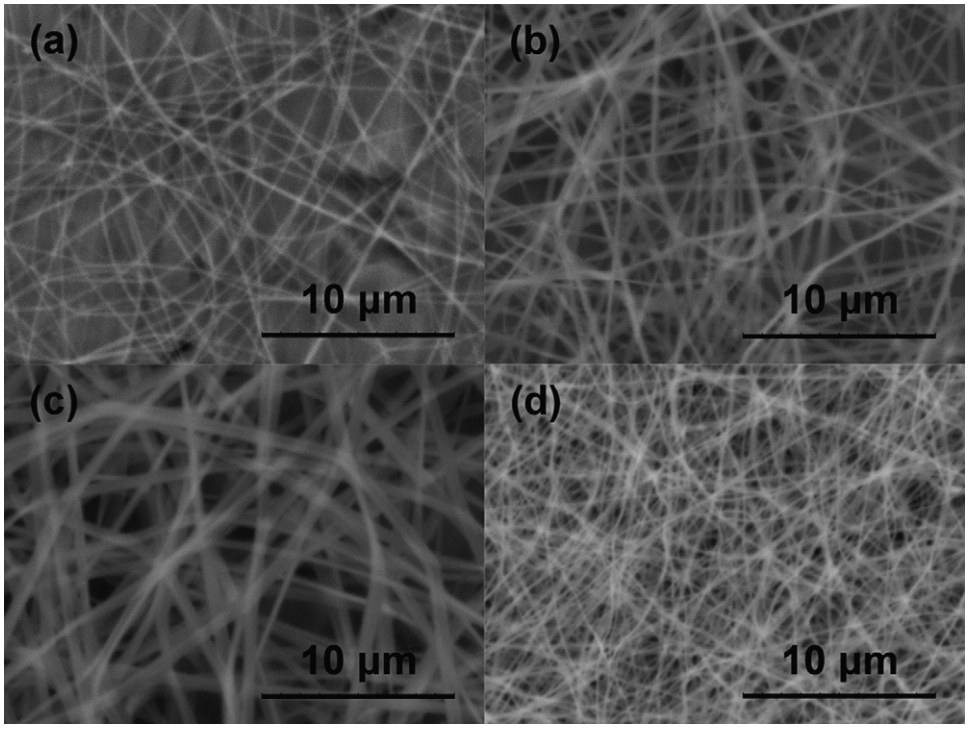

Fig. 2. (a–c) SEM images of $RE(CF_3COO)_3$/PVP composite fibers; (d) SEM image of calcined fibers corresponding to the precursor fibers in Fig. 1(b).

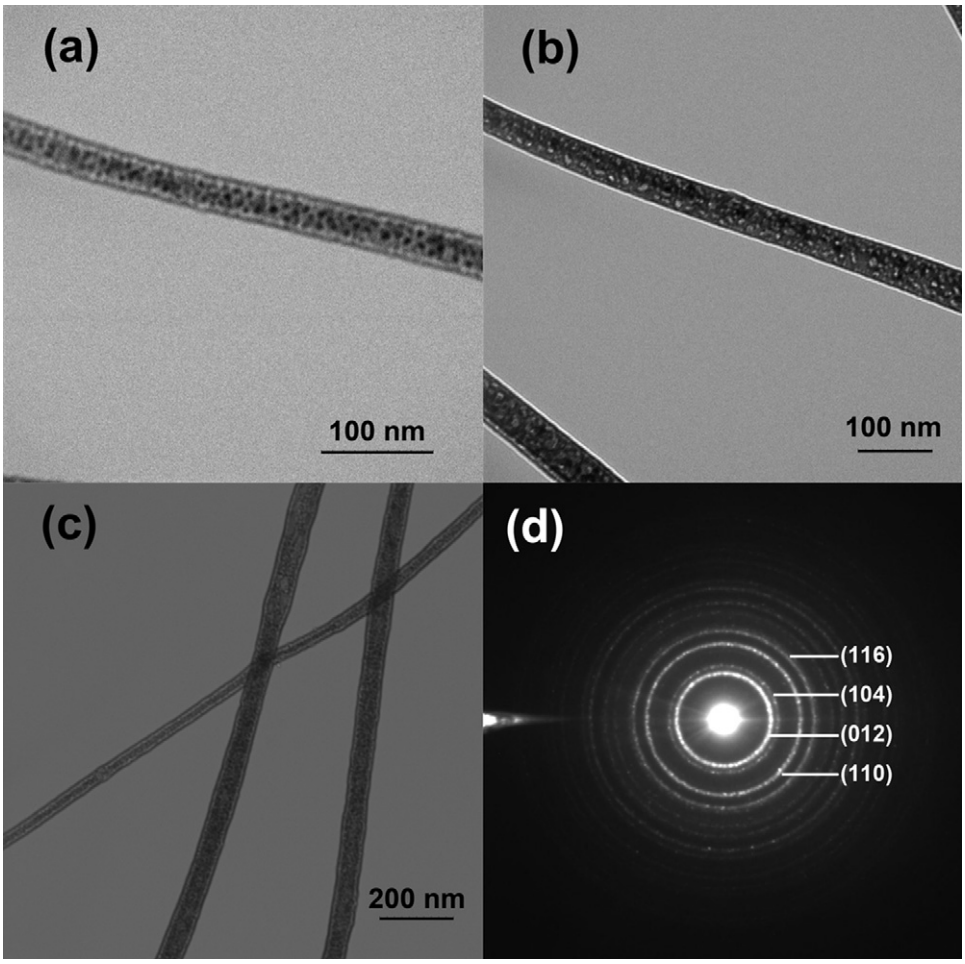

Fig. 3. TEM images of YOF:Ln^{3+} nanofibers: (a) inorganic/PVP = 2.5, sintered at 600 °C in air for 3 h; (b) inorganic/PVP = 2.5, sintered at 600 °C in air for 24 h; (c) inorganic/PVP = 0.5, sintered at 600 °C in air for 3 h. (d) The SAED pattern of YOF:Ln^{3+} nanofibers.

at a lower mass ratio gave rise to the formation of thinner fibers. It should be pointed out that a suitable weight ratio of $RE(CF_3COO)_3$/PVP is important for the formation of slender and uniform YOF fibers. If the trifluoroacetate mass ratio is too high (trifluoroacetate/PVP > 5.0), the precursor fibers will hardly be obtained. On the contrary, the sintered products will be incompact and fragile during the calcination when the inorganic content is too low (trifluoroacetate/PVP < 0.1).

TEM images shown in Fig. 3(a–c) indicate that the YOF:Ln^{3+} nanofibers have been packed with nanocrystals, and the SAED pattern in Fig. 3(d) confirms that the fibers are polycrystalline. The product in Fig. 3(a) was obtained by annealing the precursor at 600 °C for 3 h, while the sample in Fig. 3(b) at 600 °C for 24 h. The nanocrystals in Fig. 3(a) are smaller than those in Fig. 3(b), implying that the nanocrystals grew larger as the duration of calcination prolonged. When the $RE(CF_3COO)_3$/PVP mass ratio decreased to 0.5, comparing with that in Fig. 3(a), the average nanocrystal size in the fibers of Fig. 3(c) became smaller. The diffraction rings in Fig. 3(d) can be easily indexed to the (0 1 2), (1 0 4), (1 1 0), and (1 1 6) planes of the rhombohedral YOF, respectively. The corresponding lattice layer separations are d_1 = 3.1 Å, d_2 = 2.7 Å, d_3 = 1.9 Å, and d_4 = 1.6 Å, respectively.

Fig. 4(a) shows the FTIR spectra of $RE(CF_3COO)_3$/PVP composite fibers and YOF:Ln^{3+} fibers. The CO_2 contributed to the band at about 2360 cm^{-1}. The bands at 1658 cm^{-1} and 1209 cm^{-1} resulted from C=O group and C–N group in PVP, respectively. The $-COO^-$ and C–F groups of trifluoroacetate generated the bands at 1469 cm^{-1} and 1145 cm^{-1}, respectively. After the precursor fibers were calcined at 600 °C in air, the peaks at 1658, 1469, 1209, and 1145 cm^{-1} disappear from the FTIR spectrum of YOF:Ln^{3+}, which indicates that the organic components in the fibers have been burn out. A wide absorption band below 650 cm^{-1} is assigned to YOF, implying further the formation of YOF.

The TGA curve of $RE(CF_3COO)_3$/PVP composite fibers is shown in Fig. 4(b). There is a slight (<5%) weight loss with increasing the temperature from 50 °C to 200 °C due to the release of water and ethanol absorbing on the sample. A steep descent between 250 °C and 350 °C is probably attributed to the decomposition of trifluoroacetate and PVP. Yttrium oxyfluoride formed when the annealing temperature was set between 400 °C and 600 °C. The PVP could not be decomposed thoroughly until 600 °C. However, a further heat treatment could give rise of the transformation from oxyfluoride to oxide.

2.2. UC fluorescence properties and UC mechanism of YOF:Ln^{3+} nanofibers

Under continuous 980 nm light excitation, the emission spectra of the doped YOF fibers were recorded at room temperature. In the YOF:Ln^{3+} system, Yb^{3+} ions acting as sensitizers absorbed 980 nm photons. Adjacent Tm^{3+} or Er^{3+} ions got the energy from these Yb^{3+} ions via energy transfer. Here, the pump power density of 980 nm laser was about 140 mW/cm^2, the spectral resolution was 5.0 nm, and the voltage of photomultiplier tube (PMT) was 400 V.

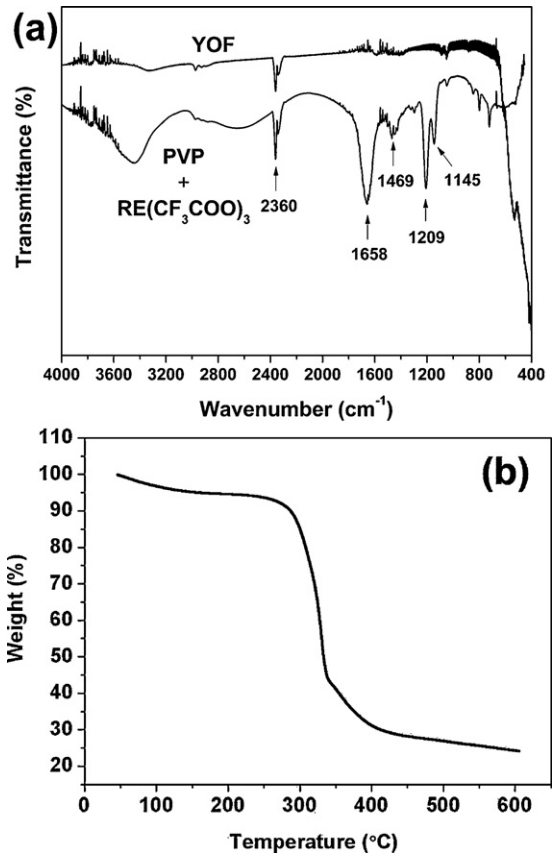

Fig. 4. (a) FTIR transmittance spectra of $RE(CF_3COO)_3$/PVP composite fibers and YOF:Ln^{3+} fibers; (b) TGA curve of $RE(CF_3COO)_3$/PVP composite fibers.

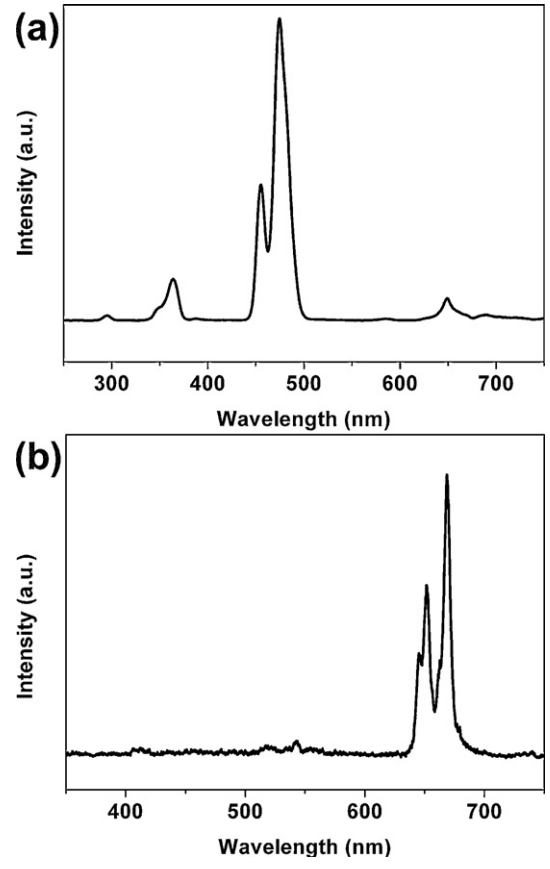

Fig. 5. UC emission spectrum of YOF:Ln^{3+} fibers (λ_{ex} = 980 nm): (a) YOF:Yb^{3+},Tm^{3+}; (b) YOF:Yb^{3+},Er^{3+}.

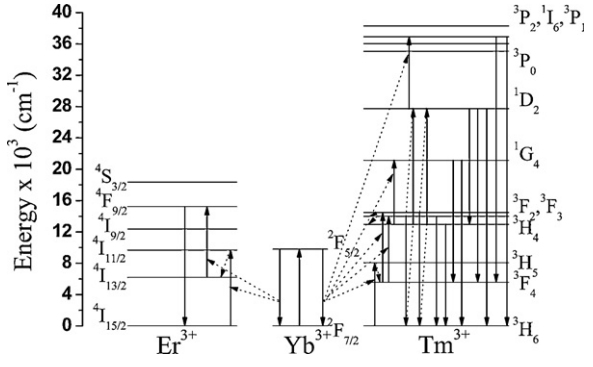

Fig. 6. Proposed UC mechanisms in YOF:Yb^{3+},Tm^{3+} and YOF:Yb^{3+},Er^{3+} fibers under 980 nm excitation.

In the $Y_{0.795}Yb_{0.2}Tm_{0.005}OF$ sample, intense blue UC light could be observed by naked eye. As shown in Fig. 5(a), the emission peaks of Tm^{3+} ions correspond to the following transitions: $^1I_6 \rightarrow {}^3H_6$ (~294 nm), $^1I_6 \rightarrow {}^3F_4$ (~347 nm), $^1D_2 \rightarrow {}^3H_6$ (~364 nm), $^1D_2 \rightarrow {}^3F_4$ (~455 nm), $^1G_4 \rightarrow {}^3H_6$ (~474 nm) and $^1G_4 \rightarrow {}^3F_4$ (~649 nm).

In the YOF:Yb^{3+},Tm^{3+} system, Yb^{3+} ions acting as sensitizer were excited by 980 nm light, shown in Fig. 6 Yb^{3+} ions absorbed 980 nm photons and then depopulated from $^2F_{5/2}$ to $^2F_{7/2}$ level. Adjacent Tm^{3+} ions got energy from these Yb^{3+} ions via energy transfer (ET). The Tm^{3+} ions could be excited from the ground state $^3H_6$ to the $^3F_2$ and $^1G_4$ levels by two and three successive ET, respectively. The $^3H_4$ level was populated by the nonradiative relaxation from the $^3F_2$ or $^3F_3$ level. Large energy mismatch (about 3500 cm^{-1}) between $^2F_{5/2} \rightarrow {}^2F_{7/2}$ and $^1G_4 \rightarrow {}^1D_2$ transitions made it unavailable for populating the $^1D_2$ level via ET from Yb^{3+} to Tm^{3+}, $^2F_{5/2} \rightarrow {}^2F_{7/2}$ (Yb^{3+}): $^1G_4 \rightarrow {}^1D_2$ (Tm^{3+}). In Tm^{3+} ions, it was the cross relaxation process between energy levels ($^3F_2$/$^3F_3$ + $^3H_4 \rightarrow {}^3H_6$ + $^1D_2$) that played a key role in populating the $^1D_2$ level. Thereafter, the $^3P_2$ level could be populated by $^2F_{5/2} \rightarrow {}^2F_{7/2}$ (Yb^{3+}):$^1D_2 \rightarrow {}^3P_2$ (Tm^{3+}), and then relaxed to $^1I_6$ level which exhibited the emissions at 294 nm and 347 nm.

Under 980 nm excitation, the UC properties of YOF:Yb^{3+},Er^{3+} were also studied. Red UC fluorescence from YOF:Yb^{3+},Er^{3+} was observed. The emission bands centered at 379 nm, 404 nm, 517 nm, 542 nm and 668 nm correspond to the transitions from the excited states $^4G_{11/2}$, $^2H_{9/2}$, $^2H_{11/2}$, $^4S_{3/2}$, $^4F_{9/2}$ to the ground state $^4I_{15/2}$, respectively. Fig. 5(b) shows visible spectrum of $Y_{0.76}Yb_{0.2}Er_{0.04}OF$ fibers. The red emission corresponds to the transition from the excited states $^4F_{9/2}$ to the ground state $^4I_{15/2}$.

The proposed UC mechanism for the YOF:Yb^{3+},Er^{3+} system is shown in Fig. 6. The $^4F_{9/2}$ level of Er^{3+} ions were populated from ground level $^4I_{15/2}$ by the processes of an ET $^2F_{5/2} \rightarrow {}^2F_{7/2}$ (Yb^{3+}):$^4I_{15/2} \rightarrow {}^4I_{11/2}$ (Er^{3+}), a fast nonradiative relaxation from the $^4I_{11/2}$ to the $^4I_{13/2}$ level, and another ET $^2F_{5/2} \rightarrow {}^2F_{7/2}$ (Yb^{3+}):$^4I_{13/2} \rightarrow {}^4F_{9/2}$ (Er^{3+}), where the $^4I_{13/2}$ level was acting as a bridge. The ions in the $^4F_{9/2}$ state relaxed radioactively to ground state giving vivid red emission.

3. Conclusion

Ln^{3+} doped oxyfluoride nanofibers with tunable diameters were fabricated successfully by using electrospinning method combining with high-temperature calcination in air. The as-prepared $RE(CF_3COO)_3$/PVP composite fibers had lengths of several millimeters. The composite fibers were sintered at 500 °C and 600 °C in air, yielding orthorhombic $Y_7O_6F_9$:Ln^{3+} and rhombohedral YOF:Ln^{3+}, respectively. The annealed sample presented 1D morphology. The calcined nanofibers were polycrystalline and

were packed by YOF:Ln^{3+} nanocrystals. The nanocrystals grew larger when the calcination duration was prolonged or the mass ratio of trifluoroacetate/PVP increased. The FTIR transmittance spectra and TGA curve of the annealed nanofibers indicated that the organic content was burned out after the calcination process. Under the excitation of 980 nm laser, YOF:Yb^{3+},Tm^{3+} nanofibers exhibited intense blue UC fluorescence, while YOF:Yb^{3+},Er^{3+} nanofibers emitted red UC light.

4. Experimental

4.1. Sample preparation

All the chemicals were used as received without further purification. Y_2O_3, Yb_2O_3, Tm_2O_3, Er_2O_3 (purity $\geq$ 99.99%), and nitric acid were supplied by Shanghai Chemical Reagent Company. Trifluoroacetic acid (TFA) and PVP (Mw $\approx$ 1,300,000) were purchased from Aldrich Company.

Solution I was prepared by dissolving Y_2O_3 (0.88 mmol) and Yb_2O_3 (0.22 mmol) in deionized water (1 mL) and TFA (0.6 mL). The mixture was put in water bath at 50 °C subsequently. Solution II was prepared by dissolving 0.4 g PVP in 7 mL of ethanol and stirred for 6 h. The solutions I and II were mixed together. Then amount of aqueous solution containing 5.5 μmol $Tm(NO_3)_3$ or 44 μmol $Er(NO_3)_3$ was added in the mixed solution. After magnetic stirring for 2 h, the ethanol solution of trifluoroacetate/PVP acting was obtained as the precursor solution for electrospinning.

The precursor solution was employed to fabricate fibers by using electrospinning method. The operation voltage was switched to 15.0 kV. The distance between the syringe tip and collector was 12 cm. The non-woven mat consisted of composite fibers was obtained after an electrospinning process and preserved carefully in a desiccator free from humidity.

The as-fabricated mat was calcined at 600 °C in air. The calcination temperature rose from room temperature and the rising rate was 5 °C min^{-1}. After the sample cooled down to room temperature naturally, it was collected carefully and preserved in a desiccator.

4.2. Measurements and characterization

XRD analysis was performed by using an X-ray diffractometer (mode Rigaku RU-200b) with nickel-filtered Cu Kα radiation (λ = 1.54056 Å). The size and morphology of the fibers produced before and after calcination process were characterized by using SEM (Hitachi TM-1000). JEOL-2000ex TEM was employed to record the TEM images and selected area electron diffraction (SAED) images. Fourier transform infrared spectra of KBr powder-pressed pellets were recorded on a Fourier transform spectrometer (Perkin-Elmer, spectrum 1). Thermogravimetric analysis, carried out under a heating rate of 5 °C min^{-1} in air, was performed by a thermal analyzer (Perkin-Elmer PYIS 1). UC fluorescence spectra were recorded by a Hitachi F-4500 fluorescence spectrophotometer with a 980 nm diode laser acting as the excitation source.

Acknowledgements

This work was supported by the National High Technology Research and Development Program of China (863 Program: 2009AA03Z309) and the National Natural Science Foundation of China (NNSFC) (grants 10874058, 51072065, and 60908031).

References

[1] F. Zhang, D.Y. Zhao, ACS Nano 3 (2009) 159–164.
[2] L.Y. Wang, P. Li, Y.D. Li, Advanced Materials 19 (2007) 3304–3307.
[3] J. Hu, T.W. Odom, C.M. Lieber, Accounts of Chemical Research 32 (1999) 435–445.
[4] G.G. Li, C.X. Li, C.M. Zhang, Z.Y. Cheng, Z.W. Quan, C. Peng, J. Lin, Journal of Materials Chemistry 19 (2009) 8936–8943.
[5] H. Kind, H.Q. Yan, B. Messer, M. Law, P.D. Yang, Advanced Materials 14 (2002) 158–160.
[6] Y.C. Kong, D.P. Yu, B. Zhang, W. Fang, S.Q. Feng, Applied Physics Letters 78 (2001) 407–409.
[7] Y.N. Xia, P.D. Yang, Y.G. Sun, Y.Y. Wu, B. Mayers, B. Gates, Y.D. Yin, F. Kim, Y.Q. Yan, Advanced Materials 15 (2003) 353–389.
[8] C. Jiang, F. Wang, N. Wu, X. Liu, Advanced Materials 20 (2008) 4826–4829.
[9] S. Ramakrishna, K. Fujihara, W.E. Teo, T. Yong, Z.W. Ma, R. Ramaseshan, Materials Today 9 (2006) 40–50.
[10] W.E. Teo, S. Ramakrishna, Nanotechnology 17 (2006) R89–R106.
[11] D. Li, Y.N. Xia, Advanced Materials 16 (2004) 1151–1170.
[12] Z.M. Huang, Y.Z. Zhang, M. Kotaki, S. Ramakrishna, Composites Science and Technology 63 (2003) 2223–2253.
[13] W. Sigmund, J. Yuh, H. Park, V. Maneeratana, G. Pyrgiotakis, A. Daga, J. Taylor, J.C. Nino, Journal of the American Ceramic Society 89 (2006) 395–407.
[14] L. Wang, Y. Li, Nano Letters 6 (2006) 1645–1649.
[15] R. Ramaseshan, S. Ramakrishna, S. Sundarrajan, R. Jose, Journal of Applied Physics 102 (2007) 111101.
[16] A. Greiner, J.H. Wendorff, Angewandte Chemie International Edition 46 (2007) 5670–5703.
[17] H. Zhang, H. Song, H. Yu, X. Bai, S. Li, G. Pan, Q. Dai, T. Wang, W. Li, S. Lu, X. Ren, H. Zhao, Journal of Physical Chemistry C 111 (2007) 6524–6527.
[18] X. Li, B. Liu, Z. Li, Q. Li, Y. Zou, D. Liu, D. Li, B. Zou, T. Cui, G. Zou, Journal of Physical Chemistry C 113 (2009) 4737–4740.
[19] M. Li, J. Zhang, H. Zhang, Y. Liu, C. Wang, X. Xu, Y. Tang, B. Yang, Advanced Functional Materials 17 (2007) 3650–3656.
[20] J.W. Stouwdam, F.C.J.M. van Veggel, Nano Letters 2 (2002) 733–737.
[21] B. Dong, H. Song, H. Yu, H. Zhang, R. Qin, X. Bai, G. Pan, S. Lu, F. Wang, L. Fan, Q. Dai, Journal of Physical Chemistry C 112 (2008) 1435–1440.
[22] A. Kumar, R. Jose, K. Fujihara, J. Wang, S. Ramakrishna, Chemistry of Materials 19 (2007) 6536–6542.
[23] D. Li, Y. Xia, Nano Letters 3 (2003) 555–560.
[24] G. Li, Z. Hou, C. Peng, W. Wang, Z. Cheng, C. Li, H. Lian, J. Lin, Advanced Functional Materials 20 (2010) 3446–3456.
[25] Z. Hou, C. Li, P. Ma, G. Li, Z. Cheng, C. Peng, D. Yang, P. Yang, J. Lin, Advanced Functional Materials 21 (2011) 2356–2365.
[26] Z. Hou, G. Li, H. Lian, J. Lin, Journal of Materials Chemistry 22 (2012) 5254–5276.
[27] Z. Hou, P. Yang, C. Li, L. Wang, H. Lian, Z. Quan, J. Lin, Chemistry of Materials 20 (2008) 6686–6696.
[28] H. Song, H. Yu, G. Pan, X. Bai, B. Dong, X.T. Zhang, S.K. Hark, Chemistry of Materials 20 (2008) 4762–4767.
[29] L. Xu, H. Song, B. Dong, Y. Wang, X. Bai, G. Wang, Q. Liu, Journal of Physical Chemistry C 113 (2009) 9609–9615.
[30] P. Du, L. Song, J. Xiong, Z. Xi, D. Jin, L. Wang, Nanotechnology 22 (2011) 035602.
[31] Y. Liu, D. Tu, H. Zhu, R. Li, W. Luo, X. Chen, Advanced Materials 22 (2010) 3266–3271.
[32] M. Haase, H. Schäfer, Angewandte Chemie International Edition 50 (2011) 5808–5829.
[33] J. Hao, Y. Zhang, X. Wei, Angewandte Chemie International Edition 50 (2011) 6876–6880.
[34] J. Wang, F. Wang, C. Wang, Z. Liu, X. Liu, Angewandte Chemie International Edition 50 (2011) 10369–10372.
[35] F. Wang, X. Liu, Chemical Society Reviews 38 (2009) 976–989.
[36] F. Wang, R. Deng, J. Wang, Q. Wang, Y. Han, H. Zhu, X. Chen, X. Liu, Nature Materials 10 (2011) 968–973.
[37] C.M. Bender, J.M. Burlitch, D. Barber, C. Pollock, Chemistry of Materials 12 (2000) 1969–1976.
[38] R. Yan, Y. Li, Advanced Functional Materials 15 (2005) 763–770.